ADVANCED MATERIALS
www.advmat.de

Materials Views
www.MaterialsViews.com

Hydrothermal Route for Cutting Graphene Sheets into Blue-Luminescent Graphene Quantum Dots

By *Dengyu Pan,* Jingchun Zhang, Zhen Li,* and *Minghong Wu**

Graphene-based materials are promising building blocks for future nanodevices owing to their superior electronic, thermal, and mechanical properties as well as their chemical stability.[1–11] However, currently available graphene-based materials produced by typical physical and chemical routes, including micromechanical cleavage,[2] reduction of exfoliated graphene oxide (GO),[3] and solvothermal synthesis,[4] are generally micrometer-sized graphene sheets (GSs), which limits their direct application in nanodevices. In this context, it has become urgent to develop effective routes for cutting large GSs into nanometer-sized pieces with a well-confined shape, such as graphene nanoribbons (GNRs) and graphene quantum dots (GQDs).

Theoretical and experimental studies[5–7] have shown that narrow GNRs (width less than ca. 10 nm) exhibit substantial quantum confinement and edge effects that render GNRs semiconducting. By comparison, GQDs possess strong quantum confinement and edge effects when their sizes are down to 100 nm.[8] If their sizes are reduced to ca. 10 nm, comparable with the widths of semiconducting GNRs, the two effects will become more pronounced and, hence, induce new physical properties. Up to now, nearly all experimental work on GNRs and GQDs has focused on their electron transportation properties.[1,5–8] Little work has been done on the optical properties that are directly associated with the quantum confinement and/or edge effects.

Most GNR- and GQD-based electronic devices have been fabricated by lithography techniques, which can realize widths and diameters down to ca. 20 nm.[9,10] This physical approach, however, is limited by the need for expensive equipment and especially by difficulties in obtaining smooth edges. Alternative chemical routes can overcome these drawbacks. Moreover, surface functionalization can be realized easily. Li et al. first reported a chemical route to functionalized and ultrasmooth GNRs with widths ranging from 50 nm to sub-10 nm.[7] Very recently, Kosynkin et al. reported a simple solution-based oxidative process for producing GNRs by lengthwise cutting and unraveling of multiwalled carbon nanotube (CNT) side walls.[11] Yet, no chemical routes have been reported so far for preparing functionalized GQDs with sub-10 nm sizes. Here, we report on a novel and simple hydrothermal approach for the cutting of GSs into surface-functionalized GQDs (ca. 9.6-nm average diameter). The functionalized GQDs were found to exhibit bright blue photoluminescence (PL), which has never been observed in GSs and GNRs owing to their large lateral sizes. The blue luminescence and new UV–vis absorption bands are directly induced by the large edge effect shown in the ultrafine GQDs.

The starting material was micrometer-sized rippled GSs obtained by thermal reduction of GO sheets. Figure 1a shows a typical transmission electron microscopy (TEM) image of the pristine GSs. Their (002) interlayer spacing is 3.64 Å (Fig. 1c), larger than that of bulk graphite (3.34 Å). Before the hydrothermal treatment, the GSs were oxidized in concentrated H_2SO_4 and HNO_3. After the oxidization treatment the GSs became slightly smaller (50 nm–2 μm) and the (002) spacing slightly increased to 3.85 Å (Fig. 1c). During the oxidation, oxygen-containing functional groups, including C=O/COOH, OH, and C–O–C, were introduced at the edge and on the basal plane, as shown in the Fourier transform infrared (FTIR) spectrum (Fig. 1d). The presence of these groups makes the GSs soluble in water.

A series of more marked changes took place after the hydrothermal treatment of the oxidized GSs at 200 °C. First, the (002) spacing was reduced to 3.43 Å (Fig. 1c), very close to that of bulk graphite, indicating that deoxidization occurs during the hydrothermal process. The deoxidization is further confirmed by the changes in the FTIR and C 1s X-ray photoelectron spectroscopy (XPS) spectra. After the hydrothermal treatment, the strongest vibrational absorption band of C=O/COOH at 1720 cm^{-1} became very weak and the vibration band of epoxy groups at 1052 cm^{-1} disappeared (Fig. 1d). In the XPS C 1s spectra of the oxidized and hydrothermally reduced GSs (Fig. 2a), the signal at 289 eV assigned to carboxyl groups became weak after the hydrothermal treatment, whereas the sp^2 carbon peak at 284.4 eV was almost unchanged. Figure 2b shows the Raman spectrum of the reduced GSs. A G band at 1590 cm^{-1} and a D band at 1325 cm^{-1} were observed with a large intensity ratio I_D/I_G of 1.26.

Second, the size of the GSs decreased dramatically and ultrafine GQDs were isolated by a dialysis process. Figure 3 shows typical TEM and atomic force microscopy (AFM) images of the GQDs. Their diameters are mainly distributed in the range of 5–13 nm (9.6 nm average diameter). Their topographic heights are mostly between 1 and 2 nm, similar to those observed in functionalized GNRs with 1–3 layers.[7] More than 85% of the GQDs consist of 1–3 layers.

[*] Prof. D. Y. Pan
Institute of Nanochemistry and Nanobiology
Shanghai University
Shanghai 201800 (P. R. China)
E-mail: dypan617@shu.edu.cn
Prof. M. H. Wu, J. C. Zhang, Prof. Z. Li
Shanghai Applied Radiation Institute
Shanghai University
Shanghai 201800 (P. R. China)
E-mail: mhwu@staff.shu.edu.cn

DOI: 10.1002/adma.200902825

WILEY InterScience DISCOVER SOMETHING GREAT
© 2010 WILEY-VCH Verlag GmbH & Co. KGaA, Weinheim

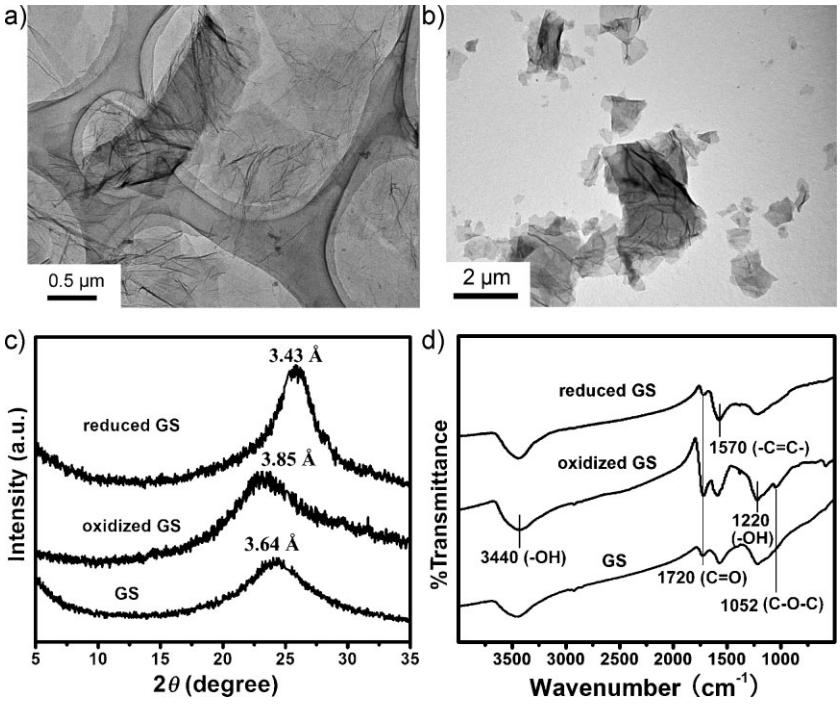

Figure 1. a,b) TEM images of the pristine (a) and oxidized (b) GSs. c,d) XRD patterns (c) and FTIR spectra (d) of the pristine, oxidized, and hydrothermally reduced GSs.

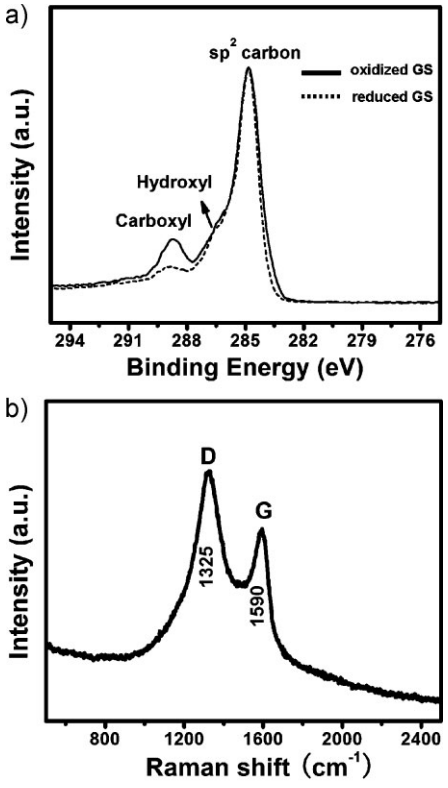

Figure 2. a) XPS C 1s spectra of the oxidized and hydrothermally reduced GSs. b) Raman spectrum of the hydrothermally reduced GSs.

The third marked change involves the UV–vis absorption of the oxidized GSs and the GQDs dispersed in water (Fig. 4a). For the oxidized GSs, a typical absorption peak at ca. 230 nm was observed, which is assigned to the $\pi \rightarrow \pi^*$ transition of aromatic sp^2 domains.[2] For the GQDs, however, besides the strong $\pi \rightarrow \pi^*$ absorption peak, a new absorption band at ca. 320 nm was also observed.

The most interesting finding is the observation of a new PL behavior. The oxidized GSs show no detectable PL even when the PL measurement is made under alkali conditions. In contrast, the GQDs emit bright blue luminescence even in neutral media (Fig. 4c). On excitation at the absorption band of 320 nm, the PL spectrum shows a strong peak at 430 nm with a Stokes shift of 110 nm (0.99 eV) (Fig. 4a). The PL quantum yield measured using quinine sulfate as a reference is 6.9%, comparable with those of reported luminescent carbon nanoparticles.[12–14] Like most luminescent carbon nanoparticles,[12–14] the GQDs also exhibit an excitation-dependent PL behavior. When the excitation wavelength is changed from 320 to 420 nm, the PL peak shifts to longer wavelengths and its intensity decreases rapidly, with the strongest peak excited at the absorption band (Fig. 4b). The PL excitation (PLE) spectrum recorded with the strongest luminescence shows two sharp peaks at 257 and 320 nm (Fig. 4c). Like the 320-nm excitation, the 257-nm excitation also induces the strongest PL at 430 nm (Fig. 4c). The 320-nm PLE peak corresponds to the 320-nm absorption band. The 257-nm PLE peak should have a corresponding absorption band that can hide in the strong background absorption from the π–π* transition. The PLE spectrum clearly demonstrates that the observed luminescence from the GQDs is directly correlated with the two new transitions at 257 and 320 nm rather than the commonly observed π–π* transition.

All these changes show that the hydrothermal treatment exerts a strong influence on the formation, microstructure, and optical properties of the GQDs. Three related fundamental issues are to be addressed. i) How are the oxidized GSs cut into the GQDs during the hydrothermal process? ii) What is the edge structure of the GQDs? iii) How do we understand the strong blue emission and the two characteristic PLE peaks of the GQDs? May the optical properties be related to the structure and chemistry of the edges?

The oxidation of CNTs is known to lead to the breaking of long CNTs into shortened CNTs and narrow GNRs,[11,15] and an unzipping mechanism has been proposed for the cutting.[11,16] During acid oxidization, epoxy groups tend to form a line on a carbon lattice and the cooperative alignment induces a rupture of the underlying C−C bonds.[16] Once an epoxy chain appears, it is energetically preferable for it to be further oxidized into epoxy pairs that then convert to more stable carbonyl pairs at room temperature.[17] Considering that the FTIR spectrum of the oxidized GSs shows a strong carbonyl signal and a very weak

© 2010 WILEY-VCH Verlag GmbH & Co. KGaA, Weinheim

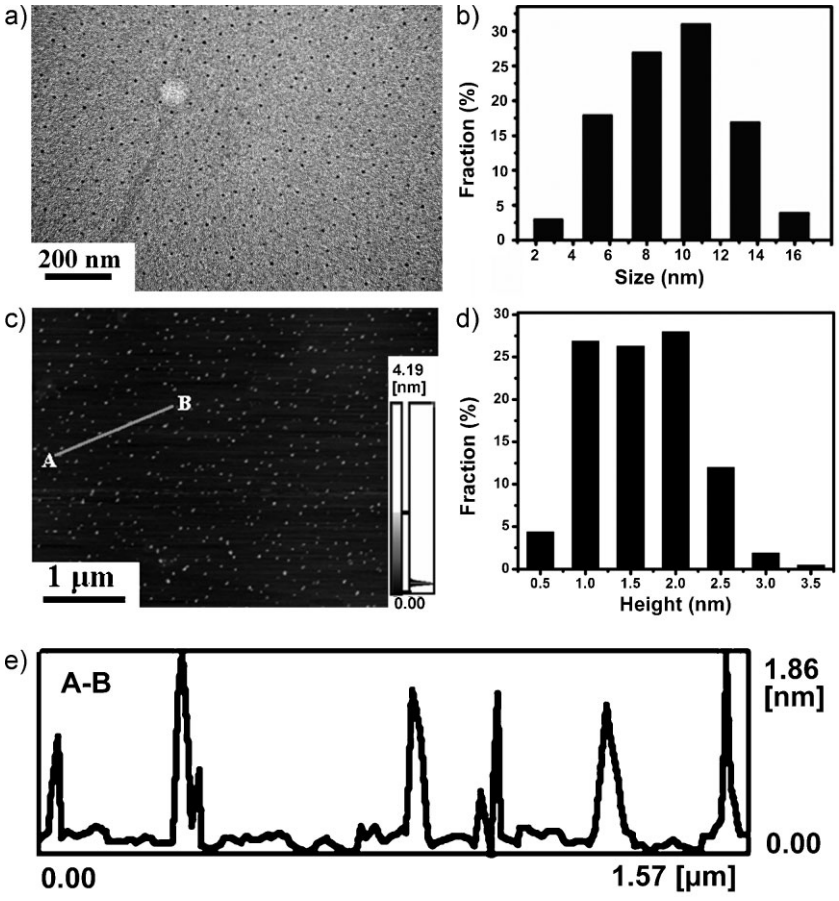

Figure 3. a) TEM image of the GQDs. b) Diameter distribution of the dots. c) AFM image of the dots deposited on freshly cleaved mica substrates. d) Height distribution of the dots. Height $\leq$1 nm, one layer; ca. 1.5 nm, two layers; ca. 2.0 nm, three layers. More than 85% of the GQDs: 1–3 layers. e) Height profile along the line A–B in (c).

epoxy signal, we propose that mixed epoxy chains composed of fewer epoxy groups and more carbonyl groups may exist in the oxidized GSs, as illustrated in Scheme 1a (left). The presence of these linear defects makes the GSs fragile and readily attacked. Some ultrafine pieces surrounded by the mixed epoxy lines and/or edges may further break up during the hydrothermal deoxidization process, by which the bridging O atoms in the epoxy lines are removed, and thus the GQDs form eventually (Scheme 1a, right).

The periphery of GSs generally consists of zigzag and chair edges. In a chemically derived GS, free edges coexist with functionalized edges. Radovic and Bockrath established a structural model for GSs and proposed that free zigzag sites are carbene-like, with a triplet ground state being most common, whereas free armchair sites are carbyne-like, with a singlet ground state most common.[18] The carbene centers at zigzag sites are stabilized by virtue of localization of itinerant π electrons through σ–π coupling.[18] We propose structural models of GQDs in acidic and alkali media based on the reversible protonation of carbene-like zigzag sites[18,19] and the reversible protonation of oxygen-containing functional groups (Scheme 1b). The protonation based on the formation of the electron-donor/acceptor complex between the delocalized π-electron system with H^+[20] is ruled out just because the observed PL is not associated with the delocalized π-electron system.

Strong PL was found in surface-functionalized CNTs,[21,22] nanodiamonds,[23,24] and carbon nanoparticles.[12–14] One class of luminescent carbon nanostructures, including shortened CNTs[22] and amorphous[12] and crystalline[13,14] carbon nanoparticles, display some similar PL behaviors, such as excitation-dependent PL and the strongest emission in the blue range, although they differ in their carbon skeleton. The similar PL behaviors suggest that they share the same luminescence origin. The most likely luminescent species is emissive surface defects, which were first proposed tentatively by Sun et al.[13] However, what chemical species the emissive defects are remains unknown.

The luminescent GQDs are added to the luminescent carbon family. We propose that the luminescence may originate from free zigzag sites with a carbene-like triplet ground state. The GQDs emit strong luminescence most likely because there is a high concentration of free zigzag sites owing to the small diameter (ca. 9.6 nm). In contrast, the previously reported large GSs are unable to emit efficiently, which can be correlated with their large lateral sizes (few micrometers or larger). The absorption, visible PL, and PLE spectra of triplet carbene in diarylmethylmethylenes have been reported and the PLE spectra with two sharp peaks are similar to that observed in the GQDs.[25]

The proposed PL mechanism based on the emissive free zigzag sites is further supported by the observed pH-dependent PL (Fig. 4d). Under alkaline conditions, the GQDs emit strong PL whereas, under acidic conditions, the PL is nearly completely quenched. If pH is switched repeatedly between 13 and 1, the PL intensity varies reversibly. This reversible phenomenon can be well understood based on the proposed structural models (Scheme 1b) and the PL mechanism of the GQDs. Under acidic conditions, the free zigzag sites of the GQDs are protonated, forming a reversible complex between the zigzag sites and H^+. Thus the emissive triple carbene state is broken and becomes inactive in PL. However, under alkaline conditions, the free zigzag sites are restored, thereby leading to the restoration of PL.

Carbenes have two electronic configurations in ground states: triplet and singlet. For the triplet state described as $\sigma^1\pi^1$, the two orbitals σ and π are singly occupied, while for the singlet state σ^2, two nonbonding electrons are paired in the σ orbital, leaving the π orbital vacant. The carbene ground-state multiplicity is related to

WILEY InterScience DISCOVER SOMETHING GREAT
© 2010 WILEY-VCH Verlag GmbH & Co. KGaA, Weinheim

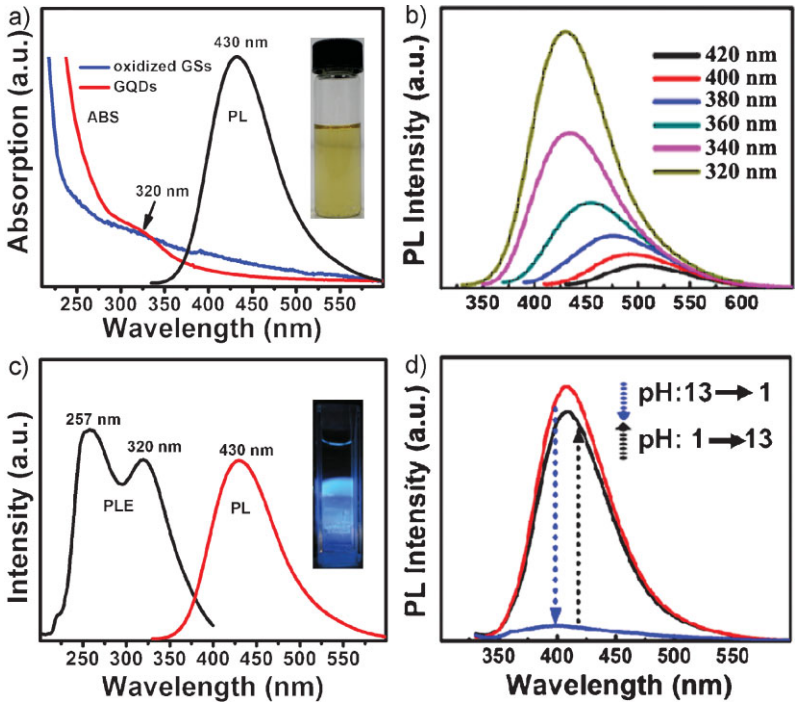

Figure 4. a) UV–vis absorption (ABS, red) and PL (at 320 nm excitation) spectra of the GQDs dispersed in water; UV–vis absorption (ABS, blue) spectrum of oxidized GSs. Inset: Photograph of the GQD aqueous solution taken under visible light. b) PL spectra of the GQDs at different excitation wavelengths. c) PLE spectrum with the detection wavelength of 430 nm and PL spectrum excited at 257 nm. Inset: Photograph of the GQD aqueous solution taken under UV light in a fluorescence spectrophotometer. d) pH-dependent PL spectra when pH is switched between 13 and 1.

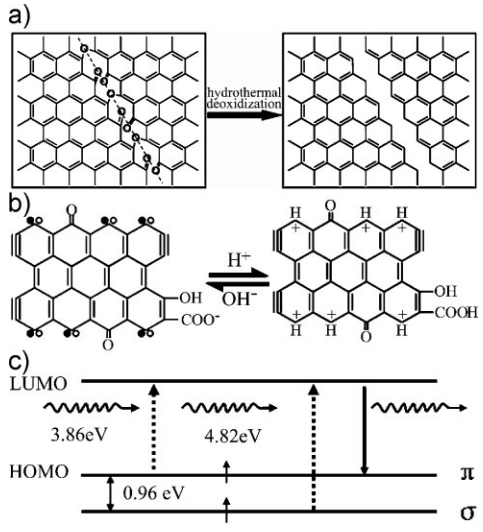

Scheme 1. a) Mechanism for the hydrothermal cutting of oxidized GSs into GQDs: a mixed epoxy chain composed of epoxy and carbonyl pair groups (left) is converted into a complete cut (right) under the hydrothermal treatment. b) Models of the GQDs in acidic (right) and alkali (left) media. The two models can be converted reversibly depending on pH. The pairing of σ (•) and π (○) localized electrons at carbene-like zigzag sites and the presence of triple bonds at the carbyne-like armchair sites are represented. c) Typical electronic transitions of triple carbenes at zigzag sites observed in the optical spectra (Fig. 4).

energy difference (δE) between the σ and π orbitals. Hoffmann determined that for a triplet ground state, δE should be below 1.5 eV.[26,27] Because the triple carbenes are most common at zigzag edges,[18] the two electronic transitions of 320 nm (3.86 eV) and 257 nm (4.82 eV) observed in the PLE spectra can be regarded as transitions from the σ and π orbitals (highest occupied molecular orbitals, HOMOs) to the lowest unoccupied molecular orbital (LUMO), as demonstrated in Scheme 1c. The δE is thus determined to be 0.96 eV, within the required value (<1.5 eV) for triple carbenes, which suggests that the assignment of the two transitions is reasonable. Because the two transitions are directly correlated with the observed blue PL, the blue emission is the irradiation decay of activated electrons from the LUMO to the HOMO.

In conclusion, we have developed a hydrothermal method for cutting preoxidized GSs into ultrafine GQDs with strong blue emission. The cutting mechanism may involve the complete breakup of mixed epoxy chains composed of fewer epoxy groups and more carbonyl groups under hydrothermal conditions. Structural models for the GQDs in acidic and alkali media have been established. The blue luminescence may originate from free zigzag sites with a carbene-like triplet ground state described as $\sigma^1\pi^1$. The study of the quantum confinement effect of the GQDs is currently under way. The discovery of the new PL from GQDs may expand the application of graphene-based materials to other fields such as optoelectronics and biological labeling.

© 2010 WILEY-VCH Verlag GmbH & Co. KGaA, Weinheim

Experimental

Preparation: GO sheets were prepared from natural graphite powder by a modified Hummers method [28,29]. GSs were obtained by thermal deoxidization of GO sheets in a tube furnace at 200–300 °C for 2 h with a heating rate of 5 °C min^{-1} in a nitrogen atmosphere. GSs (0.05 g) were oxidized in concentrated H_2SO_4 (10 mL) and HNO_3 (30 mL) for 15–20 h under mild ultrasonication (500 W, 40 kHz). The mixture was then diluted with deionized (DI) water (250 mL) and filtered through a 0.22-μm microporous membrane to remove the acids. Purified oxidized GSs (0.2 g) were re-dispersed in DI water (40 mL) and the pH was tuned to 8 with NaOH. The suspension was transferred to a poly(tetrafluoroethylene) (Teflon)-lined autoclave (50 mL) and heated at 200 °C for 10 h. After cooling to room temperature, the resulting black suspension was filtered through a 0.22-μm microporous membrane and a brown filter solution (yield ca. 22%) was separated. The colloidal solution still contained some large graphene nanoparticles (50–200 nm) that emitted weak blue fluorescence. So, the colloidal solution was further dialyzed in a dialysis bag (retained molecular weight: 3500 Da) overnight and GQDs that were strongly fluorescent through the bag were obtained with a yield of ca. 5%.

Characterization: AFM images were taken using a SPM-9600 atomic force microscope. TEM observations were performed on a JEOL JEM-2010F electron microscope operating at 200 kV. X-ray powder diffraction (XRD) patterns were obtained with a Rigaku D/max-2500 using Cu Kα radiation. Absorption and fluorescence spectra were recorded at room temperature on a Hitachi 3100 spectrophotometer and a Hitachi 7000 fluorescence spectrophotometer, respectively. FTIR spectra were recorded with a Bio-Rad FTIR spectrometer FTS165. Raman spectra were recorded on a Renishaw in plus laser Raman spectrometer with $\lambda_{exc} = 785$ nm. XPS C 1s spectra were collected using a Kratos Axis Ultra DLD X-ray photoelectron spectrometer.

Acknowledgements

This work is supported by the Natural Science Foundation of China (10774118), the Shanghai Leading Academic Discipline Project (no. S30109), and the Science and Technology Commission of Shanghai Municipality (no. 08520512200).

Received: August 17, 2009
Published online: December 10, 2009

[1] A. K. Geim, K. S. Novoselov, *Nat. Mater.* **2007**, *6*, 183.
[2] K. S. Novoselov, A. K. Geim, S. V. Morozov, D. Jiang, Y. Zhang, S. V. Dubonos, I. V. Grigorieva, A. A. Firsov, *Science* **2004**, *306*, 666.
[3] D. Li, M. B. Müller, S. Gilje, R. B. Kaner, G. G. Wallace, *Nat. Nanotech.* **2008**, *3*, 101.
[4] M. Choucair, P. Thordarson, J. A. Stride, *Nat. Nanotech.* **2008**, *4*, 30.
[5] Y.-W. Son, M. L. Cohen, S. G. Louie, *Phys. Rev. Lett.* **2006**, *97*, 216803.
[6] X. Wang, Y. Ouyang, X. Li, H. Wang, J. Guo, H. Dai, *Phys. Rev. Lett.* **2008**, *100*, 206803.
[7] X. Li, X. Wang, L. Zhang, S. Lee, H. Dai, *Science* **2008**, *319*, 1229.
[8] L. A. Ponomarenko, F. Schedin, M. I. Katsnelson, R. Yang, E. W. Hill, K. S. Novoselov, A. K. Geim, *Science* **2008**, *320*, 356.
[9] M. Y. Han, B. Ozyilmaz, Y. B. Zhang, P. Kim, *Phys. Rev. Lett.* **2007**, *98*, 206805.
[10] C. Stampfer, J. Güttinger, F. Molitor, D. Graf, K. Ensslin, *Appl. Phys. Lett.* **2008**, *92*, 012102.
[11] D. V. Kosynkin, A. L. Higginbotham, A. Sinitskii, J. R. Lomeda, A. Dimiev, B. K. Price, J. M. Tour, *Nature* **2009**, *458*, 872.
[12] A. B. Bourlinos, A. Stassinopoulos, D. Anglos, R. Zboril, M. Karakassides, E. P. Giannelis, *Small* **2008**, *4*, 455.
[13] Y.-P. Sun, B. Zhou, Y. Lin, W. Wang, K. A. S. Fernando, P. Pathak, M. J. Meziani, B. A. Harruff, X. Wang, H. F. Wang, P. J. G. Luo, H. Yang, M. E. Kose, B. L. Chen, L. M. Veca, S.-Y. Xie, *J. Am. Chem. Soc.* **2006**, *128*, 7756.
[14] J. Zhou, C. Booker, R. Zhou, X. Li, T. Sham, X. Sun, Z. Ding, *J. Am. Chem. Soc.* **2007**, *129*, 744.
[15] A. Lu, T. Iverson, K. Shelimov, C. B. Huffman, F. Rodriguez-Macias, Y.-S. Shon, T. R. Lee, D. T. Colbert, R. E. Smalley, *Science* **1998**, *280*, 1253.
[16] J.-L. Li, K. N. Kudin, M. J. McAllister, R. K. Prud'homme, I. A. Aksay, R. Car, *Phys. Rev. Lett.* **2006**, *96*, 176101.
[17] Z. Li, W. Zhang, Y. Luo, J. Yang, J. Hou, *J. Am. Chem. Soc.* **2009**, *131*, 6320.
[18] L. R. Radovic, B. Bockrath, *J. Am. Chem. Soc.* **2005**, *127*, 5917.
[19] A. Mehta, E. J. Nelson, S. M. Webb, J. K. Holt, *Adv. Mater.* **2009**, *21*, 102.
[20] a) J. C. Ma, D. A. Dougherty, *Chem. Rev.* **1997**, *97*, 1303. b) A. M. Miguel, J. A. Menéndez, E. Fuente, D. Suárez, *J. Phys. Chem. B* **1998**, *102*, 5595.
[21] S. Ju, W. P. Kopcha, F. Papadimitrakopoulos, *Science* **2009**, *323*, 1319.
[22] J. E. Riggs, Z. Carroll, D. L. Guo, Y.-P. Sun, *J. Am. Chem. Soc.* **2000**, *122*, 5879.
[23] V. N. Mochalin, Y. Gogotsi, *J. Am. Chem. Soc.* **2009**, *131*, 4594.
[24] A. Nish, J.-Y. Hwang, J. Doig, R. J. Nicholas, *Nat. Nanotechnol.* **2007**, *2*, 640.
[25] A. M. Trozzolo, W. A. Gibbons, *J. Am. Chem. Soc.* **1967**, *89*, 239.
[26] D. Bourissou, O. Guerret, F. P. Gabba, G. Bertrand, *Chem. Rev.* **2000**, *100*, 39.
[27] R. Hoffmann, *J. Am. Chem. Soc.* **1968**, *90*, 1475.
[28] Y. Xu, H. Bai, G. Lu, C. Li, G. Shi, *J. Am. Chem. Soc.* **2008**, *130*, 5856.
[29] D. Pan, S. Wang, B. Zhao, M. Wu, H. Zhang, Y. Wang, Z. Jiao, *Chem. Mater.* **2009**, *21*, 3137.

WILEY InterScience® DISCOVER SOMETHING GREAT
© 2010 WILEY-VCH Verlag GmbH & Co. KGaA, Weinheim